Peer-reviewed version available at Coatings 2018, 8, 326; doi:10.3390/coatings8090326

Article

Porosity characterization of cold sprayed stainless steel coating using three-dimensional X-ray microtomography

Yingying Wang [1], Jérôme Adrien [2] and Bernard Normand [2,*]

[1] College of Chemistry and Chemical Engineering, Southwest Petroleum University, Chengdu 610500, China; yingyingwanglyon@126.com (Y.W.)
[2] Université de Lyon, INSA de Lyon, MATEIS CNRS UMR 5510, 69621 Villeurbanne, France; jerome.adrien@insa-lyon.fr (J.A.) ; bernard.normand@insa-lyon.fr (B.N.)
* Correspondence: bernard.normand@insa-lyon.fr (B.N.); Tel.: + +33-04-72-43-62-87

Abstract: Cold gas-dynamic spray (cold spray) is an evolving coating deposition and restoration technology in which particles are deposited above the sonic speed. This paper presents the non-destructive three-dimensional characterization of cold sprayed stainless steel coating. The visualization of coating morphology and volumetric porosity, and the analyses of porosity size and spatial distributions confirmed that dense stainless steel coating with non-connected, micron-sized gradient porosity is successfully produced by cold spray. The suitability of X-ray tomography for characterizing cold sprayed coatings is assessed.

Keywords: X-ray tomography; cold spray; porosity; stainless steel; three-dimensional imaging

1. Introduction

In recent years, there has been a significant advance in the applications of cold gas-dynamic spray (also named cold spray) for producing coatings and restoration by high velocity (300~1200 m/s) impact of solid metallic powder particles [1]. Cold spray was originally developed in the mid-1980s at the Institute of Theoretical and Applied Mechanics of the Siberian Division of the Russian Academy of Science in Novosibirsk by Professor Anatolii Papyrin [2]. In this process, powder particles are accelerated by the supersonic gas jet at a temperature that is always lower than the melting point of the deposited material, forming coatings from particles in the solid state. The adhesion of particles in this process is due to their kinetic energy upon impact, and the bonding of particles is attributed to the extremely high strain-rate (up to 10^9 s^{-1}) plastic deformation and adiabatic shear instabilities that occur at the interface [3–5]. Because of the low temperature involved, the deleterious defects of oxidation, phase transformation, decomposition, grain growth and other problems inherent to conventional thermal spray can be minimized or eliminated. However, the incompletely bonded interfaces between the deposited particles may result in porosity and micro-cracks.

Probably the property of most concern of cold sprayed coatings is their porosity as it is directly related to coating quality and performance. In some cold spray operations, porosity is essential. For example, the hydroxyapatite coatings used for prosthetic implants depend on the open-pore structure for attachment to natural bone tissue [6,7]. On the other hand, certain properties could be inferior because of the presence of porosity more than a specific amount. Since corrosion protection is partly based on the shielding of the substrate from an aggressive corrosive environment, if the porosity allows a direct path to the substrate, corrosion damage of structure is predictable [8,9].

A numerous techniques are available to measure porosity but the most popular one for cold sprayed coatings (as well as for all kinds of thermal sprayed coatings) is optical microscopy or scanning electron microscopy (SEM) coupled with image analysis. Besides porosity, this procedure allows microstructure, thickness, interfaces, cracks and contamination characterizations, and chemical composition analysis when combined with Energy Dispersive Spectrometer (EDS). However, there are some problems of metallographic observations, which we cannot sidestep. Firstly, optical (or electron) microscopy is a destructive test. A coupon is produced using the specified spray parameters and then destroyed in the preparation including sectioning, cleaning, mounting grinding and polishing prior to microscopic inspection [10]. Since then, the porosity of a part of product, instead of the porosity of the product is normally determined. The frequency of testing varies according to the need. Not in all cases, a single qualifying sample is sufficient. In addition, for each test specimen, a great quantity of non-overlapping view fields should be analyzed in order to get an average result (for example, 20 required in ASTM E1920 [11]). Another issue is that the metallographic preparation could induce adverse influence to the specimen by detaching particles or smearing material over voids. Secondly, this is an area measurement, which reliability is based on that the area porosity obtained in 2D is essentially equal to the volumetric porosity (3D) [12] as long as the pores are small and uniformly distributed. However, even though satisfying results with high precision and low bias are obtained from statistical analysis, the total porosity of the deposit does not have significant meaning for many applications. More crucial information about the morphology and distribution of porosity in three-dimension (open, closed, tortuosity and connected pores to name a few) is missed. Taking the hydroxyapatite biocomposites coating again as an example, a gradient porosity level is useful as bone tissues can grow into open pores creating a mechanical hinge and eliminating the need for cements [6]. Furthermore, controlling or adjusting porosity is desired in quite a few applications. As a first step, visualization and characterization of porosity must be actualized.

The X-ray tomography, one of the useful non-destructive tools, is a capable candidate to investigate the internal properties [13–15]. The main objective of this study is to determine the opportunity of using X-ray tomography as a technique for an accurate characterization of volumetric porosity in cold sprayed coatings. Three-dimensional visualization of porosity within cold sprayed stainless steel coating using 3D X-ray tomography is presented. Quantitative information on microstructural features with respect to the size distribution and spatial distribution of porosity is obtained using open software ImageJ with the 3D image processing package Fiji.

2. Materials and Methods

Commercial atomized stainless steel 316L powder particles with nominal size ranges of 10~45 μm were used as the feedstock, which irregular morphology is shown in Figure 1. A commercial cold spray system (PCS-1000, Plasma Giken Co., Ltd., Japan) was employed. Working gas was N_2 with a pressure of 3 MPa. The main gas temperature was 950 °C. The spray distance is 30 mm. Powder feed rate is 150 g/min. The substrate is aluminum 6061 plate in order to increase absorption contrast between the coating and the substrate. A field emission scanning electron microscope (FE-SEM, Supra® 55 VP, Carl Zeiss NTS GmbH, Germany) was used to observe the cross-sectional microstructure of the coating.

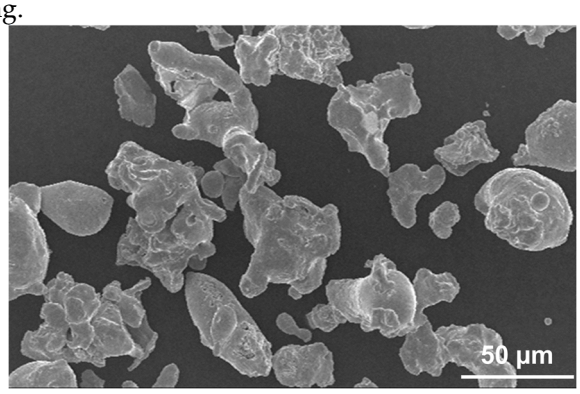

Figure 1. SEM image of irregularly shaped stainless steel 316L feedstock powder used.

X-ray tomography consists in acquiring a series of X-ray radiographs of a sample that rotates step by step around an axis perpendicular to the incident beam. The spatial density distribution is then reconstructed by using a standard filtered back-projection algorithm [16]. Inner microstructure observation of the coating was performed using a standard laboratory tomography designed by the company RX Solutions LTD. A very high resolution (compared to currently available cone beam laboratory systems) is achieved in this lab kit by using a new Hammamatsu X-ray Source. It achieves a spot size of 0.7 μm when using a W filament and this size can even be reduced further by using a LaB_6 cathode (0.25 μm). The X-ray source was operated with the LaB_6 cathode at a voltage of 100 kV. The detector was a Hamamatsu CMOS Flat Panel with a pixel size of 50 μm. The samples were scanned at a voxel size of 1.8 μm. Each scan consisted in 1200 projections with an averaging of 5 radiographs for each.

3. Results

Figure 2 shows cross–sectional SEM micrographs of the cold sprayed stainless steel 316L coating. It can be found that the deposited particles present plastic deformed morphologies, and porosity is randomly distributed. On top surface, the deformation is not sufficient to fill in all the gaps between the deposited particles. The porous top layer is formed due to the absence of tamping effect of next incoming particles. Nonetheless, there are no visible micro–channels through the coating from top to the interface.

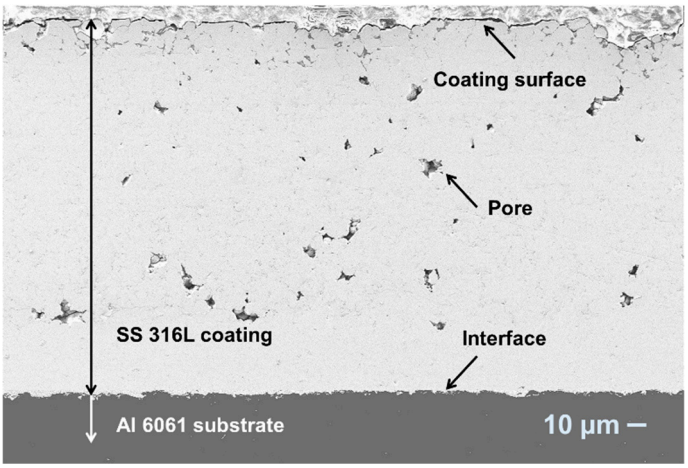

Figure 2. Cross–sectional SEM micrographs of cold sprayed stainless steel 316L coating

Figure 3 shows (a) 3D reconstructed view of cold sprayed stainless steel coating and (b) 3D rendering of the porosity's structure. In Figure 3 (a), the grey surface in the (xy) plane is top surface of coating, and the bottom is the interface, which bonds with substrate. Because of small size and small quantity of porosity, the porosity network present is a zoomed view focused in a smaller zone (Figure 3 (b)). The coating surface is connecting to the air (the continuous yellow object on the top). Pores embedded in coating (yellow objects) show irregular morphology, and larger quantity of pores located on the upper part than on the bottom part. At coating-substrate interface, porosity is also higher than main part of coating. From top surface to interface, no channels constructed from connected pores are detected.

Preprints (www.preprints.org) | NOT PEER-REVIEWED | Posted: 24 July 2018 doi:10.20944/preprints201807.0448.v1

Peer-reviewed version available at Coatings 2018, 8, 326; doi:10.3390/coatings8090326

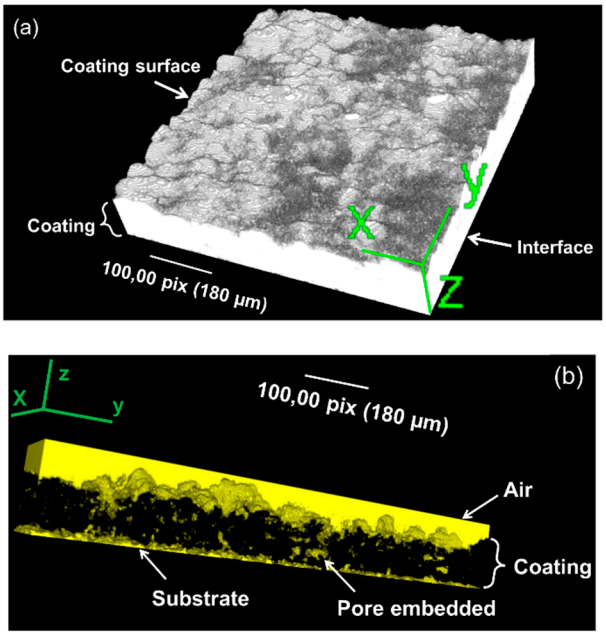

Figure 3. 3D reconstructed views of (a) cold sprayed stainless steel coating and (b) porosity network.

Figure 4 shows the tomogram image corresponding to 2D reconstructed tomographic slices of the y-axis stacking (cross-section from the view vertical to y-axis). In this absorption contrast image, the brightest intensity is found in stainless steel coating, dark grey corresponds to aluminum 6061 substrate, and black to air and pores in the coating. Coating shows the same dense cross-sectional microstructure as examined with SEM in Figure 2.

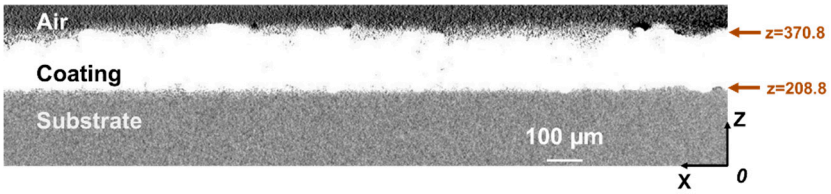

Figure 4. Reconstructed cross-section of cold sprayed SS 316L coating by tomogram image corresponding to 2D slices of the y-axis stacking

From these qualitative visualizations, 3D quantitative analyses have been performed. Typical profiles of coating density and porosity values along the three main perpendicular directions (x, y and z) are plotted in Figure 5. Coating density and porosity distribution in x direction and y direction is quite homogeneous. However, in z direction (in which the thickness is building), a gradient in the porosity is observed. At the position z=208.8 µm, there is a peak of porosity which corresponds to the coating-substrate interface. As illustrated by H. Assadi et al. [17] and Sunil Pathak et al. [18], bonding in cold spray is considered to identify with interfacial deformation, which prompts the breakup of surface oxide layers and enables the contact of metallic surfaces at atomic level. They proposed the oxide layer should be considered as a geometrical constraint to metallurgical bonding (Figure 6). Hence, the probable reason for the porosity peak at interface could be due to the native oxide layer. Before deposition the Al6061 substrate has not undergone any surface pretreatment (neither sand blasting nor polishing). During spraying, the particles impacting rough the substrate and disrupt the oxide layer. The fractured aluminum oxide layer results in noncontinuous bonding. Moreover, computational analysis demonstrates that in the initial stage of particle-substrate interaction phenomena, a thin film of particle material is deposited on the substrate. This stage depends very much on the degree of substrate surface preparation, as well as on the properties of the substrate material [19]. The native oxide layer on aluminum substrate influence the strain condition at particle-

143 substrate interface and the injection of interfacial jets from the substrate surface. This results in an
144 interfacial bonding not good enough.

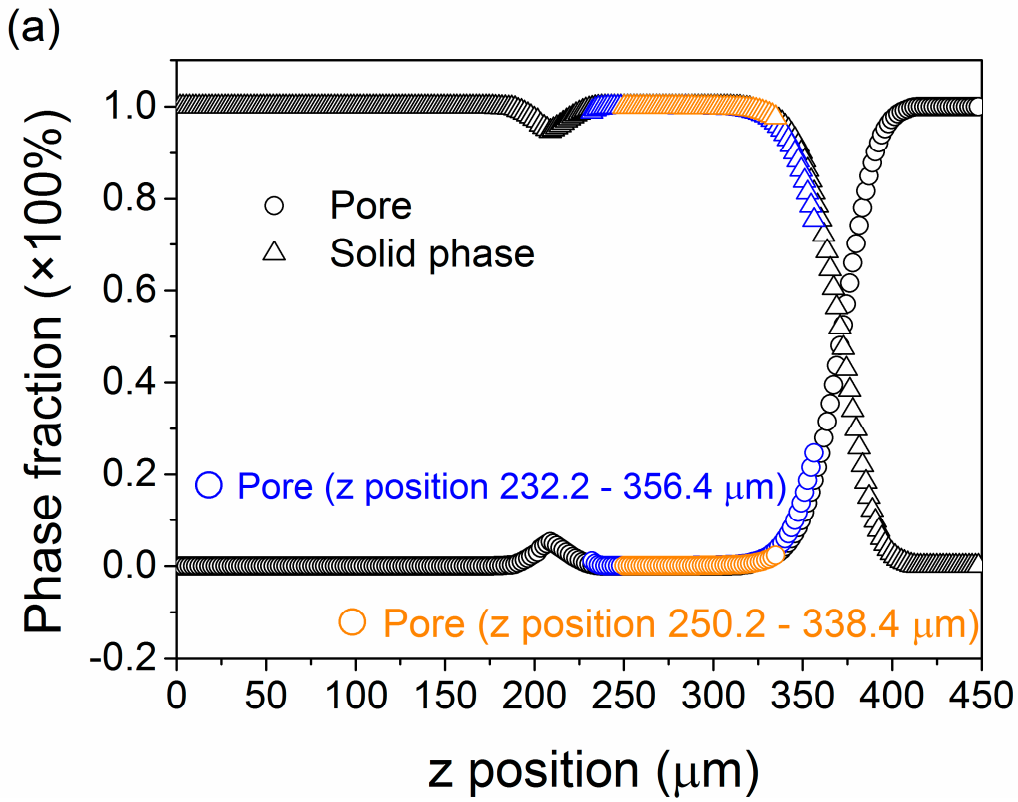

145
146

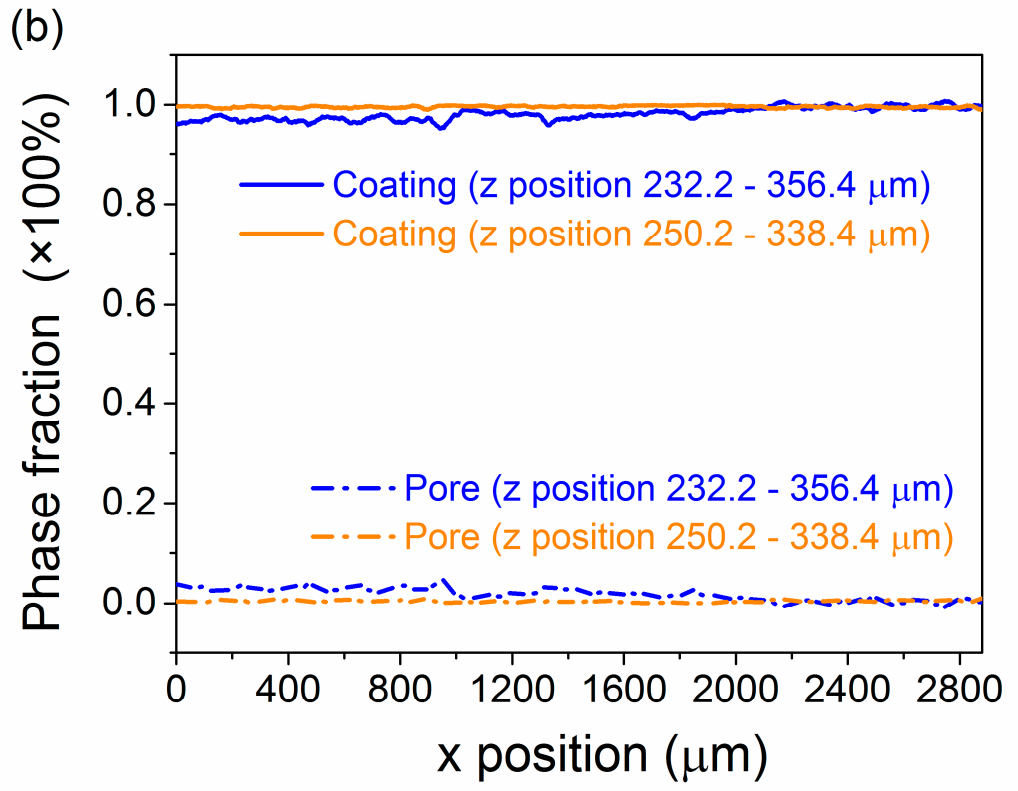

147

Peer-reviewed version available at Coatings 2018, 8, 326; doi:10.3390/coatings8090326

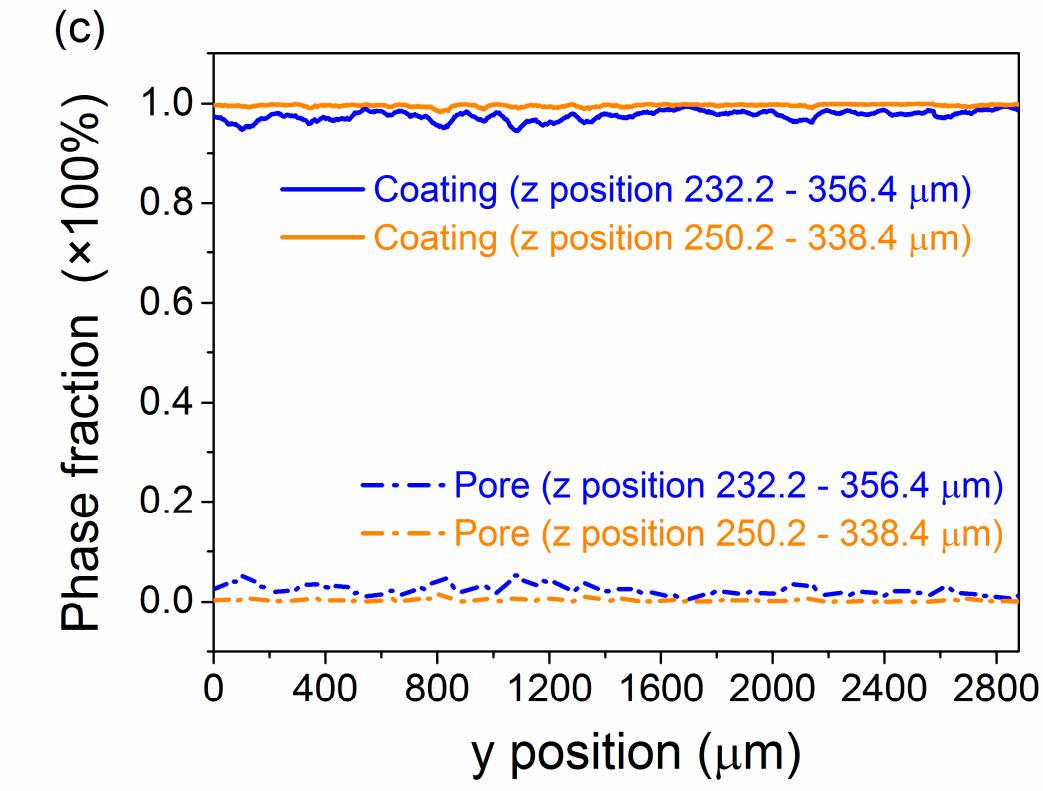

Figure 5. Porosity profiles of the cold sprayed stainless steel coating along the (a) z, (b) x and (c) y directions. Origin of coordinates (x and z) is marked in Figure 3.

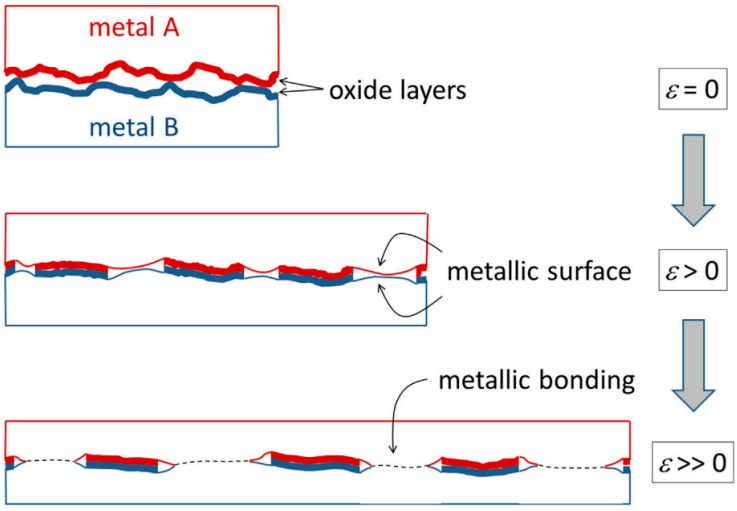

Figure 6. Schematics of interfacial plastic deformation resulting in cold welding. Under high strains, there is contact between fresh metallic surfaces and grain boundaries are formed between the two metals [17].

In Figure 5, the porosity fraction along certain axis is the porosity measured on the series of planes vertical the assigned axis based on the gray level. The average porosity reaches 1.8 % along x direction and 2.4 % along y direction (on the thickness direction, z is restricted from 208.8 μm to 370.8 μm). The inner coating layer (z ranging from 250.2 μm to 338.4 μm) is denser, and the average porosity fractions reach 0.4 % along x direction and 0.3 % along y direction.

Another important issue about porosity is the opened or closed nature of pores. The connectivity of each selected phase (solid or gaseous) can be determined by a counting procedure detecting the

3D independent objects [20]. Each object, defined as a cluster of connected voxels, can then be labeled by a different gray level on resulting tomographic slices. For the tested specimen, 19 467 non-connected objects in total are labeled in the coating, and their size distribution is calculated (Figure 7). Totally, 94.56 % of pores have the size smaller than 100 μm^3 including 44.32 % of pores smaller than 10 μm^3. The total voxel volume of pores (129 511 pixels) and total voxel volume of coating (21 490 676 pixels) result in a volumetric porosity of 0.6 %. The non-connected porosity of low level and small size promises good corrosion protection for aluminum substrate [21,22].

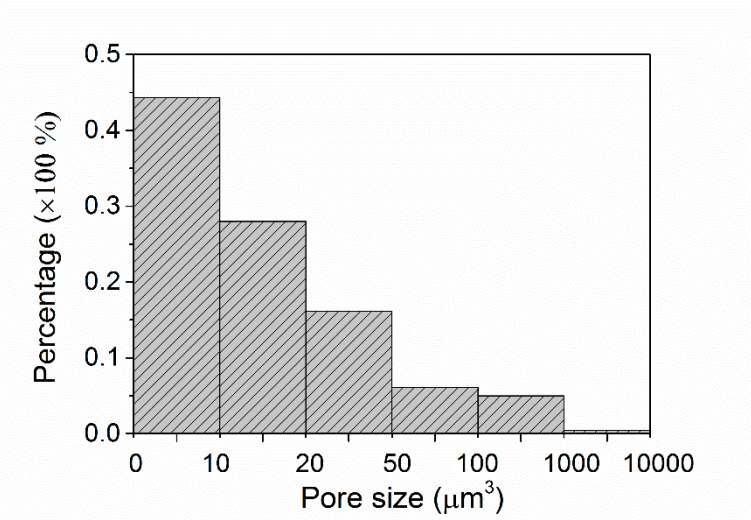

Figure 7. Pores size distribution of cold sprayed stainless steel coating.

4. Conclusions

The study reveals that cold sprayed stainless steel coating displays a micro-sized and non-connected porosity of low level. The fluctuating on porosity profile in z direction could help to identify the interface and measure coating thickness. Conversely, no porosity peak at interface is helpful to determine the spray parameters required for strong coating-substrate adhesion. Therefore, x-ray tomography technique provides three-dimensional architecture of cold sprayed coating in a non-contact and non-destructive way, and it proposes a direct visualization of voids in three-dimensional space. Microstructure, thickness, porosity fraction, pore's connectivity and size distribution are interesting parameters that can be measured from tomographic images. More work are in progress to demonstrate this opportunity and more applications on characterization of composite coatings.

Acknowledgments: This investigation is financially supported by the National Natural Science Foundation of China under grant no. 51601158 and the Qihang Science Research Foundation of Southwest Petroleum University, nNo. 2015QHZ013. The authors thankfully acknowledge Plasma Giken Co., Ltd. for providing free samples supporting the research on cold spraying at INSA de LYON.

Author Contributions: Y.W., and B.N. conceived and designed the experiments; Y.W., and J. A. performed the experiments; Y.W., J. A. and B. N. analyzed the data; Y.W. and B.N. wrote the paper.

Conflicts of Interest: The authors declare no conflict of interest.

References

1. Singh, H.; Sidhu, T. S.; Kalsi, S. B. S. Cold spray technology: future of coating deposition processes. Frat. ed Integrita Strutt. **2012**, 22, 69–84, doi:10.3221/IGF-ESIS.22.08.
2. Suhonen, T.; Varis, T.; Dosta, S.; Torrell, M.; Guilemany, J. M. Residual stress development in cold sprayed Al, Cu and Ti coatings. Acta Mater. **2013**, 61, 6329–6337, doi:10.1016/j.actamat.2013.06.033.
3. Wu, J.; Fang, H.; Yoon, S.; Kim, H.; Lee, C. The rebound phenomenon in kinetic spraying deposition. Scr. Mater. **2006**, 54, 665–669, doi:10.1016/j.scriptamat.2005.10.028.

4. Papyrin, A.; Kosarev, V.; Klinkov, S.; Alkhimov, A.; Fomin, V. M. Cold spray technology; Papyrin, A., Ed.; 1st Editio.; Elsevier, **2007**; ISBN 008046548X.
5. Assadi, H.; Gärtner, F.; Stoltenhoff, T.; Kreye, H. Bonding mechanism in cold gas spraying. Acta Mater. **2003**, 51, 4379–4394, doi:10.1016/S1359-6454(03)00274-X.
6. Lee, J. H.; Jang, H. L.; Lee, K. M.; Baek, H.-R.; Jin, K.; Hong, K. S.; Noh, J. H.; Lee, H.-K. In vitro and in vivo evaluation of the bioactivity of hydroxyapatite-coated polyetheretherketone biocomposites created by cold spray technology. Acta Biomater. **2013**, 9, 6177–87, doi:10.1016/j.actbio.2012.11.030.
7. Choudhuri, A.; Mohanty, P. S.; Karthikeyan, J. Bio-ceramic Composite Coatings by Cold Spray Technology. In Proceedings of the International Thermal Spray Conference; **2009**; pp. 391–396.
8. Marrocco, T.; Hussain, T.; McCartney, D. G.; Shipway, P. H. Corrosion performance of laser posttreated cold sprayed titanium coatings. J. Therm. Spray Technol. **2011**, 20, 909–917, doi:10.1007/s11666-011-9637-x.
9. Tao, Y.; Xiong, T.; Sun, C.; Kong, L.; Cui, X.; Li, T.; Song, G.-L. Microstructure and corrosion performance of a cold sprayed aluminium coating on AZ91D magnesium alloy. Corros. Sci. **2010**, 52, 3191–3197, doi:10.1016/j.corsci.2010.05.023.
10. ASTM standards, ASTM E2109. Test Methods for Determining Area Percentage Porosity in Thermal Sprayed Coatings. Annual Book of ASTM Standards, vol. 03.01; **2007**; Vol. 03.01;
11. ASTM standards, ASTM E1920. Standard Guide for Metallographic Preparation of Thermal Sprayed Coatings. Annual Book of ASTM Standards, vol. 03.01; **2008**;
12. Friel, J. J. Practical Guide to Image Analysis; ASM International, **2000**; ISBN 1615032371.
13. Madison, J. D.; Aagesen, L. K. Quantitative characterization of porosity in laser welds of stainless steel. Scr. Mater. **2012**, 67, 783–786, doi:10.1016/j.scriptamat.2012.06.015.
14. Maire, E.; Grenier, J.; Daniel, D.; Baldacci, A.; Klöcker, H.; Bigot, A. Quantitative 3D characterization of intermetallic phases in an Al–Mg industrial alloy by X-ray microtomography. Scr. Mater. **2006**, 55, 123–126, doi:10.1016/j.scriptamat.2006.03.066.
15. Maurel, V.; Helfen, L.; N'Guyen, F.; Koster, A.; Di Michiel, M.; Baumbach, T.; Morgeneyer, T. F. Three-dimensional investigation of thermal barrier coatings by synchrotron-radiation computed laminography. Scr. Mater. **2012**, 66, 471–474, doi:10.1016/j.scriptamat.2011.12.021.
16. Huang, R.; Ma, W.; Fukanuma, H. Effect of Particle Velocity on Cold Sprayed Stainless Steel Deposits. In Thermal Spray 2012: Proceedings of the International Thermal Spray Conference and Exposition; **2012**; pp. 594–599.
17. Youssef, S.; Maire, E.; Gaertner, R. Finite element modelling of the actual structure of cellular materials determined by X-ray tomography. Acta Mater. **2005**, 53, 719–730, doi:10.1016/j.actamat.2004.10.024.
18. Wang, Y.; Normand, B.; Suo, X.; Planche, M.-P.; Liao, H.; Tang, J. Cold-Sprayed AZ91D Coating and SiC/AZ91D Composite Coatings. Coatings **2018**, 8, 122, doi:10.3390/coatings8040122.
19. Wang, Y.; Normand, B.; Mary, N.; Yu, M.; Liao, H. Effects of ceramic particle size on microstructure and the corrosion behavior of cold sprayed SiC p /Al 5056 composite coatings. Surf. Coatings Technol. **2017**, 315, 314–325, doi:10.1016/j.surfcoat.2017.02.047.
20. Wang, Y.; Normand, B.; Mary, N.; Yu, M.; Liao, H. Microstructure and corrosion behavior of cold sprayed SiCp/Al 5056 composite coatings. Surf. Coatings Technol. **2014**, 251, 264–275, doi:10.1016/j.surfcoat.2014.04.036.
21. Elmoutaouakkil, A.; Salvo, L.; Maire, E.; Peix, G. 2D and 3D Characterization of Metal Foams Using X-ray Tomography. Adv. Eng. Mater. **2002**, 4, 803–807, doi:10.1002/1527-2648(20021014)4:10<803::AID-ADEM803>3.0.CO;2-D.